Journal of Materials Science & Surface Engineering Vol. 5 (3), 2017, pp 571-576 10.jmsse/2348-8956/5-3.5

Science IN

Contents lists available at http://www.jmsse.org/ & http://www.jmsse.in/

Journal of Materials Science and Surface Engineering

Low-temperature Thermal Exfoliation of Graphene Oxide for High Performance Supercapacitor

Sultan Ahmed[1], Md. Yasir Bhat[2], M. Rafat[1], S.A. Hashmi[2]

[1]*Department of Applied Sciences and Humanities, Jamia Millia Islamia, New Delhi-110025, India.*
[2]*Department of Physics and Astrophysics, University of Delhi, New Delhi-110007, India.*

Article history

Received: 29-Mar-2017
Revised: 03-April-2017
Available online: 20-May-2017

Keywords:
Graphene,
Thermal exfoliation,
Electrodes,
Supercapacitor

Abstract

Graphene has been successfully prepared by low temperature thermal exfoliation of graphene oxide (GO). The surface morphology, vibrational response and structural parameters have been characterized using field emission scanning electron microscopy (FESEM), X-ray diffraction (XRD), Raman Spectroscopy, Fourier transform infrared (FTIR) spectroscopy and BET surface area measurements. Results of XRD confirm the successful reduction of GO. BET measurement indicates the presence of pores in the synthesized product. Subsequently, symmetrical electric double layer capacitors (EDLCs) were fabricated with graphene oxide (GO) and thermally exfoliated graphene oxide (te-GO) electrodes, in 6 M KOH aqueous solution. These cells were analyzed using electrochemical impedance spectroscopy (EIS), cyclic voltammetry (CV) and galvanostatic charge/discharge (GCD) techniques. A decrease of a factor of four in relaxation time (τ_o) indicates a substantially higher rate performance o-GO based EDLCs, as compared to GO-based cell. The high rate capability of GO/te-GO electrodes is further confirmed from the rectangular CV shapes, up to scan rates of 1 V $s^{-1}$for GO and 3 V s^{-1} for te-GO electrodes. The te-GO based EDLC offers high capacitance (~186 F g^{-1}) and specific power (~19.84 kW kg^{-1}) in comparison to GO based cell (139 F g^{-1}, 12.05 kW kg^{-1}).The above result shows that low-temperature exfoliation of graphene oxide is possible and can be used for mass production of graphene. Also, graphene synthesized by above method, can be used profitably for supercapacitor application.

Introduction

A two-dimensional hexagonal type honeycomblattice packed carbon monolayer, called “Graphene”, has been considered to be a building block for carbonaceous materials like carbon nanotubes, graphite and fullerenes [1-2]. Graphene is the only basic member of two dimensional allotropic carbon family that forms a defect-free carbon monolayer. This has been carefully reviewed in a ‘*Carbon*Editorial’ [3]. Initially, graphene was not considered to be existing in its free state. In 2004, Novoselov and co-workers isolated a single-atom-thick layer of carbon [4]. Since then, graphene has gained the interest of researchers, and its popularity is growing continuously. However, production methods such as mechanical exfoliation [5-7], chemical vapour deposition [8-11], synthesis on SiC [12-14], bottom-up synthesis from structurally defined organic precursors [15-16], involve high cost and have limited scalability. This necessarily restricts the use of graphene for fundamental research and beyond. For mass production, reduced graphene oxide (rGO) can be a promising candidate. It may be synthesized in bulk as compared to single- or few-layer graphene. The quality is satisfactory for use in bulk material applications. Graphene oxide (GO) is prepared by oxidation of graphite using suitable oxidizing agent [17-19]. The reduction of the obtained graphene oxide to graphene may be achieved using chemical or thermal methods [20-23]. Among the two mentioned methods, due to cost-effectiveness and environment friendly approach thermal reduction of GO is preferred [24]. McAllister et al. suggest that exfoliation of GO can occur at a critical temperature of 550 °C [25]. A large number of publications in recent years have discussed the application of graphene in energy-storage electrochemical devices.

In the present work, a simple low temperature cost-effective method to synthesize thermally exfoliated graphite oxide (te-GO) is reported. Morphological and structural charcteristics as well as porosity of synthesized product have been studied using suitable characterization techniques. Electrochemical performance of synthesized product has also been studied. GO and te-GO electrodes have been used to design symmetric supercapacitor system in 6 M KOH aqueous electrolyte. The constructed symmetric device has been successfully tested using cyclic voltammetry (CV), electrochemical impedance spectroscopy (EIS) and galvanostatic charge-discharge (GCD) techniques.

Experimental

Materials

All the materials used for synthesis were of analytical grade and used without further purification. All the solutions were prepared in de-ionised (DI) water.

Preparation of Graphene oxide (GO)

Graphene oxide was synthesized according to modified Hummers method [26]. In brief the procedure is as follows. Sodium nitrate (1 g) and graphite powder (2 g) were mixed and transferred to glass beaker. Predetermined amount of concentrated

Corresponding author. Tel. +91 9540556084
E-mail address: usmanisultan@gmail.com

sulphuric acid (50 ml) was added to above beaker, and the whole solution was magnetically stirred in ice bath. After 5 min. of stirring, potassium permanganate (6 g) was very slowly added to the solution. After complete addition of the powder, the solution was stirred for another 30 minutes and afterwards the ice bath was removed. Solution was then stirred at room temperature for 1 h, followed by addition of DI water (100 ml) drop by drop. After adding DI water and stirring for 2 h, 200 ml warm DI water was added to the solution. This was followed by addition of Hydrogen peroxide (15ml, 30%). The resultant suspension was then centrifuged followed by washing with Hydrochloric acid (10%), DI water and ethanol. The resultant sample obtained was dried at 80 °C in vacuum oven overnight to obtain graphene oxide (GO).
Preparation of thermally exfoliated graphene oxide (te-GO)

GO was thermally exfoliated at ~180 °C under air atmosphere [27]. Dried GO powder was loaded in perforated alumina boat and placed in muffle furnace. Muffle furnace inner walls were wholly covered using thick aluminium foil. The temperature of the furnace was allowed to increase from room temperature. When the temperature of the furnace reached 170-180 °C, GO powder expanded into fine particles over the whole aluminium foil. These fine particles were collected and labelled as thermally exfoliated graphene oxide (te-GO).

Material characterization

The surface morphology of the synthesized product was characterized using field emission scanning electron microscopy (FESEM, MIRA3 TESCAN). For structural characterization, X-ray diffraction (XRD, Bruker) system with Cu kα radiation (λ = 1.54 A°) was used. Raman studies were performed on Horiba Yvon Raman spectrometer. To characterize the functional groups, fourier transform infrared spectra were recorded using FTIR (Perkin Elmer) spectrometer. Brunauer, Emmett and Teller (BET) surface area, pore volume and pore size of product were observed using surface area and pore size analyzer (GEMINI-V, Micrometrics).

Electrochemical characterization

To prepare supercapacitor electrodes, GO/te-GO powder, acetylene black (AB, conductive additive) and PVdF-HFP (binder) were mixed in a wt. ratio of 7:2:1. Few drops of acetone were added to the resultant mixture, to form a slurry. This slurry was coated to graphite sheets (1 cm^2). The graphite sheets containing the slurry material were dried in vacuum oven at 80 °C overnight. The dried graphite sheets were used as working electrode. 6 M KOH aqueous solution was used as electrolyte. Electric double-layer capacitors (EDLCs) cells were arranged in two-cell assembly by soaking glassy carbon filter (GCFP) in electrolyte solution and placing it between two graphite sheets. Following this configuration, two EDLCs cells were prepared-

Cell#1: G|GO|GCFP|GO|G

Cell#2: G|te-GO|GCFP|te-GO|G

(G: graphite sheet)

The relative performance of Cell#1 (comprising GO electrodes) and Cell#2 (comprising te-GO electrodes),was evaluated employing electrochemical impedance spectroscopy (EIS), Cyclic Voltammetry (CV) and galvanostatic charge-discharge (GCD) techniques. EIS studies were done in the frequency, ranging from 10 mHz to 100 kHz using electrochemical workstation (CH instruments, USA). CV measurements were done from -0.5 V to 0.5 V on the above mentioned workstation. The charge-discharge measurements were done using a charge-discharge analyzer (Arbin instruments, USA).

Results and Discussion

Electrode characterization

Figure 1 (A-C) shows the surface morphology of GO powder. The observed image clearly shows thelayer structure with stacked sheets. The arrangement of sheets is not smooth, which may be due to distorted arrangement of sheets (as a result of oxidation). However when the GO sheets are thermally expanded, most of the sheets are efficiently exfoliated (Fig. 1 (D-F)).

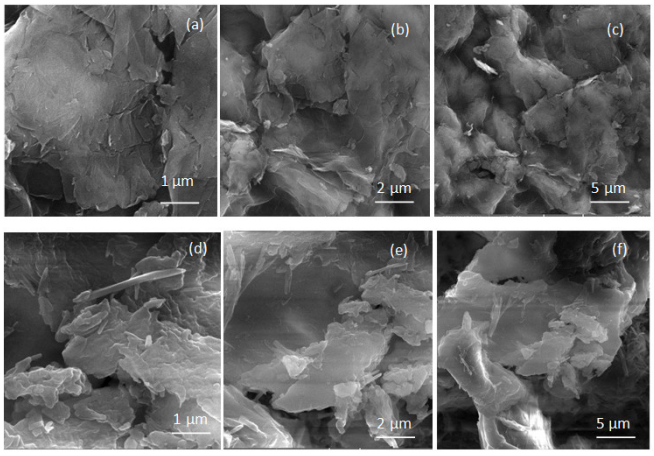

Figure 1: FESEM images of (a-c) GO and (d-f) te-GO powder

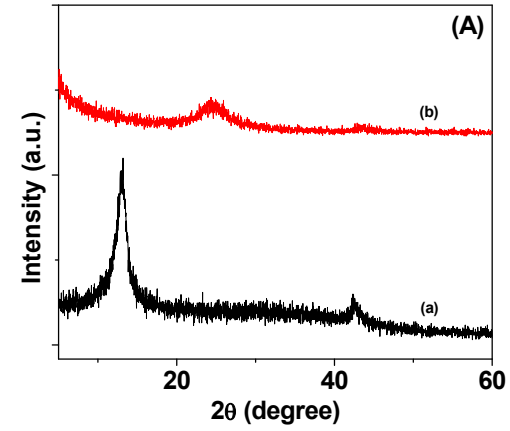

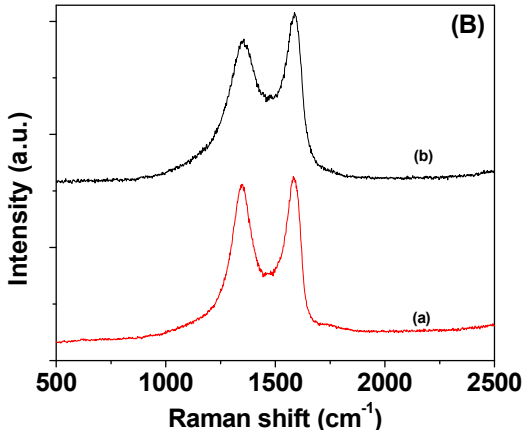

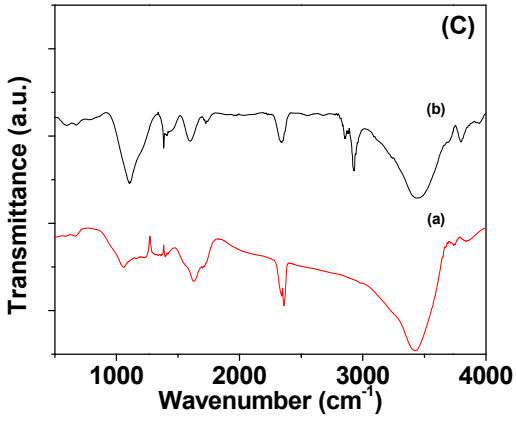

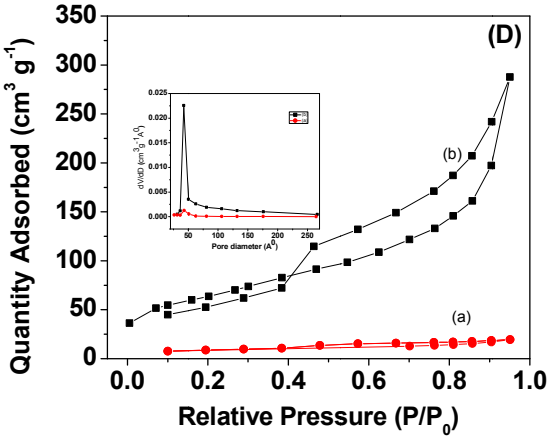

Figure 2: (A) XRD, (B) Raman, (C) FTIR and (D) N_2 adsorption isotherm of (a) GO and (b) te-GO powder

Figure 2 (A) shows the XRD pattern of GO and te-GO powder. Sharp diffraction peak at ~12.9° for GO powder indicates that graphite has been successfully oxidized. However on thermal exfoliation peak at 12.9 disappear and new weak broad diffraction peak at 24.4° is observed. The broad diffraction nature of this peak indicates amorphous nature of sample. Fig. 2 (B) shows the raman spectra of GO and te-GO powder. The spectrum contains two prominent peaks, commonly known as D and G band. Intensity ratio (I_D/I_G), which shows the ratio of defect, was calculated for GO and te-GO powder. The value observed for GO powder was greater than that for te-GO powder, indicating greater number of defects (due to aromaticity of functional groups) in GO as compared to te-GO.

Figure 2 (C) displays the FTIR spectra of GO and te-GO powder. The relatively broad peak at 3420 $cm^{-1}$and sharp peak at 1623 cm^{-1}show the presence of water molecules in GO powder, whilethe peak at 1053 cm^{-1}corresponds to C-O-C stretching. When GO powder, undergoes thermal treatment; reduction in peak at 3420 cm^{-1} and 1623 cm^{-1} is observed indicating that most of the oxygen groups have been successfully removed. Fig. 2 (D) shows the nitrogen/desorption isotherms of GO and te-GO powder. Inset of figure shows pore size distribution. The observed BET surface area, pore volume and pore size of two powder are mentioned in Table 1. BET specific surface area for GO was observed to be 11m^2 g^{-1}, which on thermal expansion increases to the value of 226 m^2 g^{-1}. This expansion in surface area can be endorsed to removal of sufficient amount of functional groups from the GO sample, resulting in generation of pores. For both GO and te-GO powder, the isotherm observed is of Type-II. This indicates the presence of mesopores in sample. The hysteresis loop has also been observed during desorption, further confirming the presence of mesopores in the interior of both GO and te-GO powder. However, BET surface area of te-GO powder is lower than theoretical limit (~3600 m^2 g^{-1}) of graphene. This shows that GO is not wholly exfoliated and there is a sufficient amount of oxygen functional groups in the sample.

Table 1: BET surface area, pore volume and pore size of GO and te-GO

Electrode Material	Bet Surface Area, S_{BET} (m^2 g^{-1})	Micropore Surface Area, S_{micro} (m^2 g^{-1})	Mesopore Surface Area, S_{meso} (m^2 g^{-1})	Micropore Volume (cm^3 g^{-1})	Total Pore Volume (cm^3 g^{-1})	Mesopore Volume (cm^3 g^{-1})	Average Pore size (A^0)
GO	28.12	1.11	27.01	.0005	.0303	.0298	43.08
teGO	226.19	12.31	213.88	.0053	.4449	.4396	78.65

Electrochemical testing

As mentioned in experimental section, two cells namely Cell#1 (comprising GO electrodes) and Cell#2 (comprising te-Go electrodes) were prepared. To evaluate their electrochemical performance, EIS, CV and GCD techniques were used. Fig. 3 (A) displays the EIS plots for the two cells.

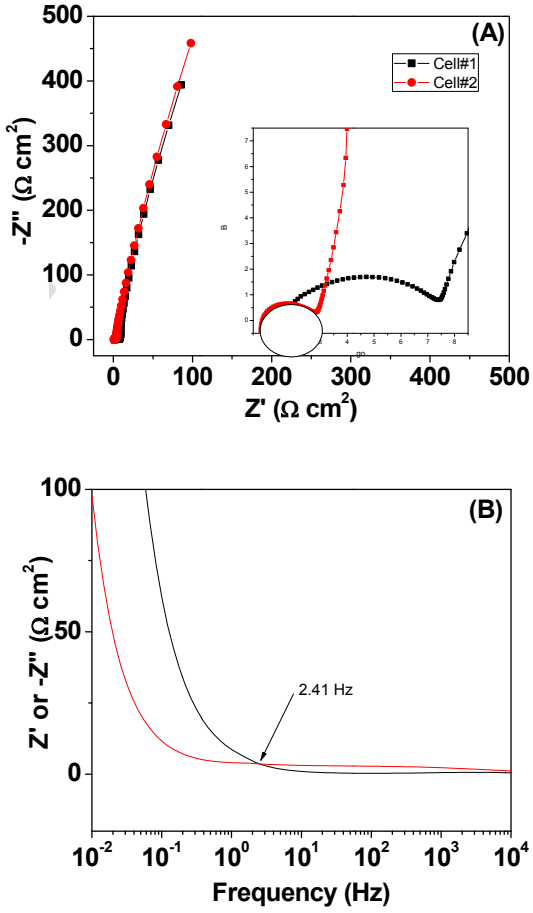

Figure 3: (A) EIS plot of Cell#1 and Cell#2 recorded at room temperature in the frequency range from 100 kHz to 10 mHz. Expanded EIS plot for cells are shown as insets. (B) Typical Bode plot for Cell#2

Table 2: Various electrical parameters of EDLC cells evaluated from the EIS plots

Cells	R_b (Ω cm^2)	R_{ct} (Ω cm^2)	C_{sp} (F g^{-1})	Response frequency, f_o (Hz)	Response time, τ_0(s)	Available specific energy, E_o (Wh kg^{-1})	Pulse Power, P_o (kWkg^{-1})
Cell#1	1.63	6.16	116.38	0.63	1.59	3.27	7.40
Cell#2	0.8	2.33	123.95	2.41	0.42	4.30	36.86

The sharply increasing pattern of the imaginary impedance (Z") in context to real part (Z') shows the capacitive nature of the cells. In different frequency regions, various parameters associated with bulk properties of electrode-electrolyte interface and electrolyte were calculated and they are listed in Table 2. The overall capacitance (C_s) of cells was evaluated at 10 mHz using the expression:

$$C = \frac{2}{\omega Z'' m} \quad (1)$$

Here, m is active mass of the single electrode material,Z" is the imaginary part of impedance andω is angular frequency of applied signal. A comparison between two prepared cells indicates that the value of specific capacitance (C_s) observed for Cell#2 (comprising te-GO electrodes) is greater than that of Cell#1 (comprising GO electrodes). The low value of C_s for Cell#1 can be attributed to its low BET surface area (11 $m^2 g^{-1}$). Also, Cell#2 shows low value of resistive component (R_b and R_{ct}) in comparison to Cell#1. This behavior can be accounted due to more conducting nature of te-GO.Inset of Fig. 3 (A) shows the difference in intermediate frequency region for the two cells. The impedance responses observed are noticeably different for the two. Cell#1 shows a larger segment in comparison to Cell#2. Larger segment indicates the resistive nature whereas smaller segment shows capacitive behavior of cells. Thus, in Cell#2 electrolyte ions encounters less resistive path as compared to Cell#1. Figure 3 (B) shows the Bode plot for Cell#2. In Bode plot, one plotsreal and imaginary part of impedance (Y-axis) as a function of log frequency (X-axis). The point at which X- and Y-axis intersect is referred to as resonant (response) frequency (f_0). Value of response time (τ_0) is the reciprocal of response frequency. Energy density (E) and pulse power density (P) were calculated using the expressions:

$$E = \frac{1}{2} C V^2 \quad (2)$$

$$P = \frac{E}{\tau_0} \quad (3)$$

where, V is working voltage window. The values obtained are listed in Table 2. A comparison of values show that Cell#2 offers low value of τ_0 and hence faster power delivery response.

Figure 4 (A-B) shows CV curves for the cells with increasing scan rates. Shape of voltammetric curve for the cells is almost rectangular indicating their capacitive behavior. However, rate capability of the two cells are different. Cell#1 shows rectangular shape up to 1 V s^{-1} whereas for Cell#2 capacitive behaviortill 3 V s^{-1} is observed. Fig. 4 (C) shows comparative CV pattern for the two cells at scan rate of 100 mV s^{-1}. As seen from the figure, CV outline for Cell#2 offers high voltammetric current and in turn high capacitance as compared to Cell#1. This is in agreement with the EIS results. The value of specific capacitance was calculated using the expression:

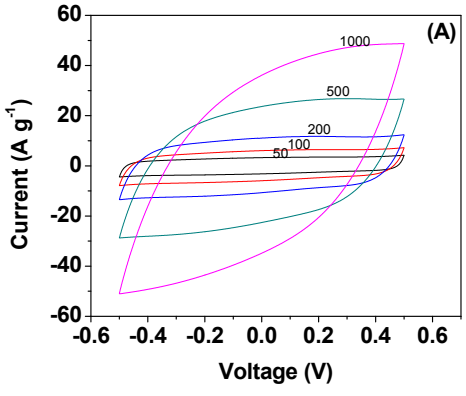

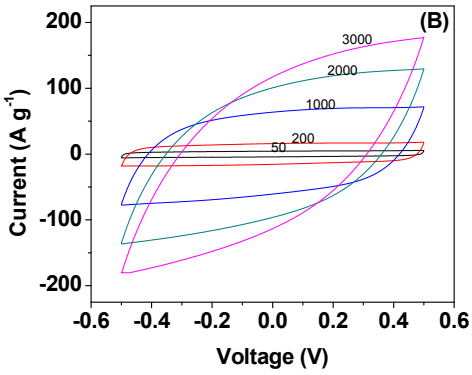

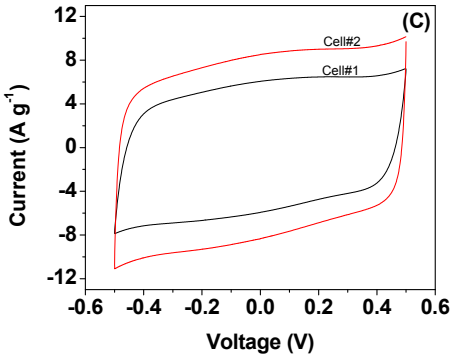

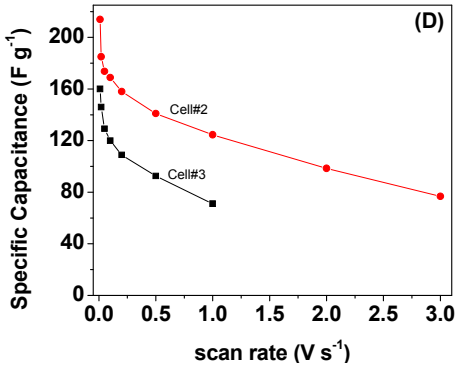

Figure 4: (A-B) CV responses of Cell#1 and Cell#2 respectively at different scan rates, (C) comparative CV patterns of two cells, (D) variation of capacitance value of Cell#1 and Cell#2 as a function of scan rates

$$C = \frac{2.I}{s.m} \quad (4)$$

Here, I is the average current of two electrode materials, m is active mass of single electrode and s is scan rate.

Figure 4 (D) shows the variation in capacitance value for the two cells as scan rate increases. The result indicates that with increase in scan rate, capacitance value decreases. This is primarily due to limited use of active sites of electrode material by electrolyte ions.

Figure 5 (A) shows the comparative charge-discharge behaviour of the cells at current density of 1 mA cm^{-2}. The discharge curves observed are almost linear, depicting capacitive nature of the cells. However, the operating voltage window for Cell#1 is less in comparison to Cell#2. The values of discharge capacitance (C_d) werecalculated from linear part of discharge curve using the expression:

$$C_d = \frac{2i}{m.\frac{\Delta V}{\Delta t}} \quad (5)$$

Here, i is constant current, m is active mass in single electrode and $\Delta V/\Delta t$ is the slope of discharge curve. The calculated values of C_d and equivalent series ratio (ESR) are listed in Table 3. A comparison of values for the two cells shows that Cell#2 offers high capacitance. This is agreement with EIS and CV results. Fig. 5 (B) shows the comparative current dependence of discharge capacitance for the cells. A gradual decrease in C_d with increase in current load, indicates that the rate capability of two cells (Cell#1 and Cell#2) is good. The specific energy (E) and power (P) of the cells were calculated using the following expressions:

$$E = \frac{C_d.V^2}{8} \quad (6)$$

$$P = \frac{V^2}{8.m.ESR} \quad (7)$$

The calculated values are listed in Table 3. It was observed that Cell#2 offers high value of power (~19.84 kW kg^{-1}) in comparison to Cell#1 (~12.05 kW kg^{-1}). Fig. 5 (C) is the ragone plot for the cells (Cell#1 and Cell#2). The shape is similar and power values calculated are high as compared to previously reported EDLCs [27].

Table 3: Charge-discharge characteristics of the capacitor cells at the current load of 1 mA cm^{-2}

Cells	ESR (Ω cm^2)	Discharge Capacitance, C_d (F g^{-1})	Specific Energy (Wh kg^{-1})	Specific Power (kW kg^{-1})
Cell#1	12	139.56	3.92	12.05
Cell#2	10	186.34	6.47	19.84

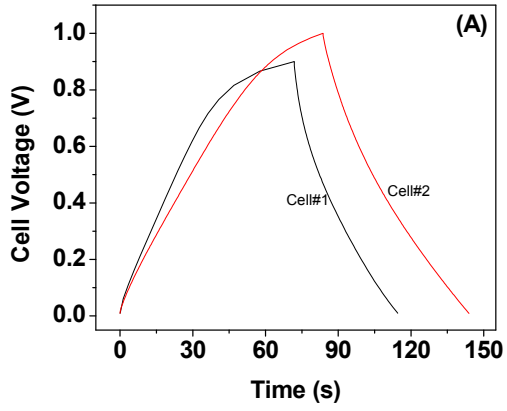

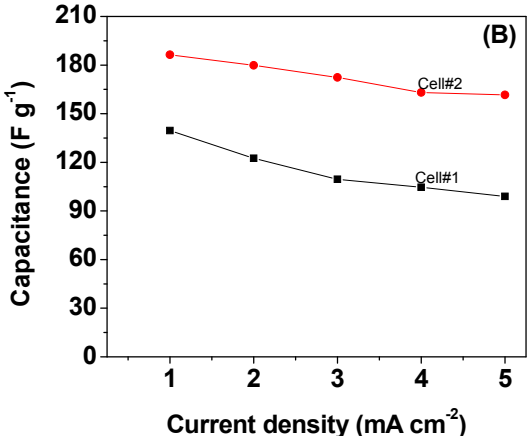

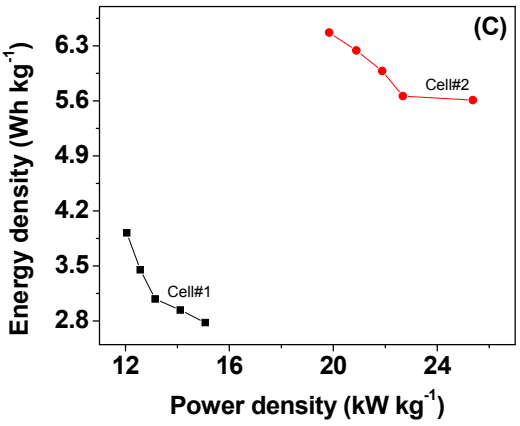

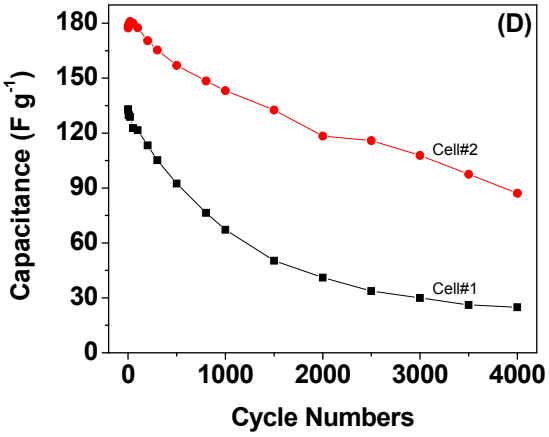

Figure 5: (A) Charge-discharge curves of two cells at constant current load of 1 mA cm^{-2}, (B) variation of discharge capacitance of cells as a function of current density, (C) Ragone plot of Cell#1 and Cell#2, (D) variation of discharge capacitance of cells at constant current load of 1 mA cm^{-2}, as a function of charge-discharge cycles

Figure 5 (D) shows the variation in specific capacitance values of the cells as a function of charge-discharge cycles. After initial fading in capacitance value for first few cycles, Cell#2 (comprising te-GO powder) shows more stability as compared to Cell#1. Greater fading in capacitance value for Cell#1 (comprising GO electrodes) is due to possible functional groups attached with the GO electrodes.

Conclusion

Summarizing the study, one may note the success of preparation method i.e. graphene oxide (GO) was prepared using modified Hummers procedure. GO sample was successfully thermally exfoliated in air atmosphere and labelled as te-GO. Results of XRD confirm successful exfoliation of GO. The results of BET analysis indicate the presence of pores in the synthesized sample.Subsequently, symmetrical EDLCs were prepared using GO/te-GO powder. Performance of the two cell was electrochemically studied. The cell comprising te-GO shows greater promise in comparison to GO cell. The preparation technique as well as cell performance are useful achievements, opening avenues of new research.

Acknowledgements

The authors gratefully acknowledge financial support received from DST, New Delhi (Sanction No. DST/TSG/PT/2009/93) & University of Delhi (11-17 Research Fund). The authors thank Dr.

Zishan H Khan, Dr. Nishant Tripathi, M. Parvaz and Zaid Ansari for their generous help in some of the characterization studies. One of us (Sultan Ahmed) is grateful to the University Grants Commission, New Delhi for providing him Junior Research Fellowship.

References

1. Zhang N, Zhang Y, Yang MQ, Tang ZR, Xu YJ. A critical and benchmark comparison on graphene, carbon nanotube, and fullerene-semiconductor nanocomposites as visible light photocatalysts for selective oxidation. Journal of catalysis. 2013, 299, 210-21.
2. Yang MQ, Zhang N, Xu YJ. Synthesis of fullerene, carbon nanotube, and graphene-TiO2 nanocomposite photocatalysts for selective oxidation: a comparative study. ACS applied materials & interfaces. 2013, 5(3), 1156-64.
3. Allen MJ, Tung VC, Kaner RB. Honeycomb carbon: a review of graphene. Chemical reviews. 2009, 110(1), 132-45.
4. Novoselov KS, Geim AK, Morozov S, Jiang D, Katsnelson M, Grigorieva I, Dubonos S, Firsov A. Two-dimensional gas of massless Dirac fermions in graphene. Nature. 2005, 438(7065), 197-200.
5. Yi M, Shen Z. A review on mechanical exfoliation for the scalable production of graphene. Journal of Materials Chemistry A. 2015, 3(22), 11700-15.
6. Chang YM, Kim H, Lee JH, Song YW. Multilayered graphene efficiently formed by mechanical exfoliation for nonlinear saturable absorbers in fiber mode-locked lasers. Applied Physics Letters. 2010, 97(21), 211102-3.
7. Martinez A, Fuse K, Yamashita S. Mechanical exfoliation of graphene for the passive mode-locking of fiber lasers. Applied Physics Letters. 2011, 99(12), 121107.
8. Chen Z, Ren W, Gao L, Liu B, Pei S, Cheng HM. Three-dimensional flexible and conductive interconnected graphene networks grown by chemical vapour deposition. Nature materials. 2011, 10(6), 424-8.
9. Yu Q, Jauregui LA, Wu W, Colby R, Tian J, Su Z, Cao H, Liu Z, Pandey D, Wei D, Chung TF. Control and characterization of individual grains and grain boundaries in graphene grown by chemical vapour deposition. Nature materials. 2011, 10(6), 443-9.
10. Reina A, Jia X, Ho J, Nezich D, Son H, Bulovic V, Dresselhaus MS, Kong J. Large area, few-layer graphene films on arbitrary substrates by chemical vapor deposition. Nano letters. 2008, 9(1), 30-5.
11. Dai B, Fu L, Zou Z, Wang M, Xu H, Wang S, Liu Z. Rational design of a binary metal alloy for chemical vapour deposition growth of uniform single-layer graphene. Nature communications. 2011, 2, 522.
12. Virojanadara C, Syväjarvi M, Yakimova R, Johansson LI, Zakharov AA, Balasubramanian T. Homogeneous large-area graphene layer growth on 6 H-SiC (0001). Physical Review B. 2008, 78(24), 245403.
13. Aristov VY, Urbanik G, Kummer K, Vyalikh DV, Molodtsova OV, Preobrajenski AB, Zakharov AA, Hess C, Hänke T, Buchner B, Vobornik I. Graphene synthesis on cubic SiC/Si wafers. Perspectives for mass production of graphene-based electronic devices. Nano letters. 2010, 10(3), 992-5.
14. Hannon JB, Tromp RM. Pit formation during graphene synthesis on SiC (0001): In situ electron microscopy. Physical Review B. 2008, 77(24), 241404.
15. Cao X, Zheng B, Rui X, Shi W, Yan Q, Zhang H. Metal Oxide-Coated Three-Dimensional Graphene Prepared by the Use of Metal–Organic Frameworks as Precursors. Angewandte Chemie International Edition. 2014, 53(5), 1404-9.
16. Dong X, Wang P, Fang W, Su CY, Chen YH, Li LJ, Huang W, Chen P. Growth of large-sized graphene thin-films by liquid precursor-based chemical vapor deposition under atmospheric pressure. Carbon. 2011, 49(11), 3672-8.
17. Dikin DA, Stankovich S, Zimney EJ, Piner RD, Dommett GH, Evmenenko G, Nguyen ST, Ruoff RS. Preparation and characterization of graphene oxide paper. Nature. 2007, 448(7152), 457-60.
18. Dreyer DR, Park S, Bielawski CW, Ruoff RS. The chemistry of graphene oxide. Chemical Society Reviews. 2010, 39(1), 228-40.
19. Marcano DC, Kosynkin DV, Berlin JM, Sinitskii A, Sun Z, Slesarev A, Alemany LB, Lu W, Tour JM. Improved synthesis of graphene oxide. ACS nano. 2010, 4(8), 4806-14.
20. Yang D, Velamakanni A, Bozoklu G, Park S, Stoller M, Piner RD, Stankovich S, Jung I, Field DA, Ventrice CA, Ruoff RS. Chemical analysis of graphene oxide films after heat and chemical treatments by X-ray photoelectron and Micro-Raman spectroscopy. Carbon. 2009, 47(1), 145-52.
21. Stankovich S, Dikin DA, Piner RD, Kohlhaas KA, Kleinhammes A, Jia Y, Wu Y, Nguyen ST, Ruoff RS. Synthesis of graphene-based nanosheets via chemical reduction of exfoliated graphite oxide. Carbon. 2007, 45(7), 1558-65.
22. Pei S, Cheng HM. The reduction of graphene oxide. Carbon. 2012, 50(9), 3210-28.
23. Gao X, Jang J, Nagase S. Hydrazine and thermal reduction of graphene oxide: reaction mechanisms, product structures, and reaction design. The Journal of Physical Chemistry C. 2009, 114(2), 832-42.
24. Paredes JI, Villar-Rodil S, Fernandez-Merino MJ, Guardia L, Martínez-Alonso A, Tascon JM. Environmentally friendly approaches toward the mass production of processable graphene from graphite oxide. Journal of Materials Chemistry. 2011, 21(2), 298-306.
25. McAllister MJ, Li JL, Adamson DH, Schniepp HC, Abdala AA, Liu J, Herrera-Alonso M, Milius DL, Car R, Prud'homme RK, Aksay IA. Single sheet functionalized graphene by oxidation and thermal expansion of graphite. Chemistry of materials. 2007, 19(18), 4396-404.
26. Suleman M, Kumar Y, Hashmi SA. High-rate supercapacitive performance of GO/r-GO electrodes interfaced with plastic-crystal-based flexible gel polymer electrolyte. Electrochimica Acta. 2015, 182, 995-1007.
27. Shivakumara S, Kishore B, Penki TR, Munichandraiah N. Symmetric Supercapacitor Based on Reduced Graphene Oxide in Non-Aqueous Electrolyte. ECS Electrochemistry Letters. 2015, 4(8), A87-9.